Towards Large Eddy Simulations of Turbulent Drag Reduction Using Sinusoidal Riblets

YULIA PEET, PIERRE SAGAUT
Université Pierre et Marie Curie - Paris 6
Institut Jean le Rond d'Alembert
4 place Jussieu, 75252 Paris Cedex 05
FRANCE

YVES CHARRON
IFP- Institut Français du Pétrole
1 et 4 Avenue du Bois Préau
92852 Rueil Malmaison Cedex
FRANCE

Abstract: A new modification to the drag reduction method using riblets is proposed, which consists of adding a sinusoidal variation to the riblet shape in spanwise direction. It is anticipated that more significant drag reduction will be achieved with sinusoidal riblets due to an oscillatory spanwise component added to the mean flow. First, Large Eddy Simulations of conventional riblet geometry consisting of straight riblets are conducted in order to validate the numerical method to be used for computational investigation of sinusoidal riblets. Summary of the previous findings on straight riblets is reported and illustrated by the results of the current simulations. Second, laminar computations of the sinusoidal riblets are documented and analyzed.

Key–Words: Drag Reduction, Riblets, Large Eddy Simulations, Turbulence, Boundary Layer

1 Introduction

Skin-friction drag reduction in a turbulent boundary layer is of immense importance in both commercial fleet and military naval applications. For a commercial fleet, improvement of the lift-to-drag ratio translates into a fuel saving. For underwater vehicles, for which 90% of the total drag is due to skin-friction, drag reduction would mean an increase of speed. Another area where drag reduction is desirable is petroleum industry, where significant pressure losses occur due to the viscous drag inside the pipelines.

There is no shortage of methods proposed in literature for reducing turbulent skin-friction drag. To name a few, there is air injection, surface heating or cooling [1], ion wind [2], introduction of foreign substances, such as polymers (long-chain molecules) [3, 4], surface-acting agents [5], compliant coating [6], microbubbles [7], fibers [8], spherical particles [9]. Another group of methods involves modification of geometry of the surface. These methods include large-eddy breaking devices (LEBU) [10, 11], surface riblets [12, 13], special kind of surface roughness [14] and high-frequency spanwise wall oscillations [15, 16]. A choice of a particular method for any given application is dictated, among other factors, by manufacturing cost, easiness of maintenance, space limitation (for example, volume required for carrying polymers on board of an aircraft or a submarine). In terms of a manufacturing cost, surface riblets is perhaps the most attractive method. However, maximum drag reduction which can be achieved using riblets is not very high, in the range of 6–8% [12], whereas, for example, a drag reduction of up to 80% can be reached in the case of a polymer injection [17]. Therefore, a combination of riblets with some other drag reducing method would be advantageous.

It was recently discovered that high-frequency spanwise oscillations of the duct wall can produce rather significant drag reduction at the optimum wall speed of $w^+ = 15$: up to 40% reported by Jung et al. [15] and up to 45% reported by Choi et al. [16]. It is worth noting that such a high values of drag reduction are obtained with an overall energy dissipation considering an external energy input. It is possible to gain a net energy saving of about 10% with the wall speed which is three times lower [18], which consequently results in lower values of drag reduction. In the current paper, we propose to modify conventional riblet geometry by adding a spanwise sinusoidal variation to the riblets. This will also add spanwise oscillatory component to the mean flow over the riblet surface, which we hope will incur additional drag-reduction benefits over conventional geometry by analogy with spanwise wall oscillations. Performing Large Eddy Simulations (LES) of a modified riblet geometry is an ultimate goal for this research. The current paper documents computational LES study of a conventional riblet geometry. Understanding mechanism of turbulent skin-friction drag reduction by straight riblets is a necessary step before investigating drag associated with sinusoidal riblets. We attempt to summarize major

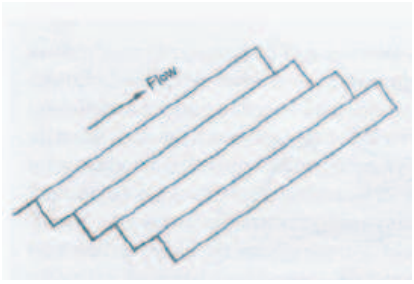

Figure 1: Three dimensional view of conventional riblets.

findings of previous researchers explaining why the drag is reduced in a straight riblet geometry and illustrate their conclusions by the results of our numerical simulations. Qualitative comparison with DNS study of the same configuration by Choi et al. [13] is also made. Laminar flow around sinusoidal riblets is then documented, showing spanwise oscillatory motion of the mean velocity.

2 Conventional and Modified Riblet Geometry

As shown in figure 1, conventional, or straight riblets, are the wall grooves aligned in the direction of the freestream flow. The riblet spanwise separation s and the shape of the cross-section are the main adjustable parameters. Previous research efforts identified V-grooves (shown in figure 1) as an optimum riblet cross-section [12], with an optimum height and spacing of about $15\nu/u_\tau$. It was further confirmed that the riblet configuration continues to remain drag reducing as long as the height and spacing of the grooves do not exceed $25\nu/u_\tau$, after which it becomes drag increasing [13, 19].

The proposed modification is to introduce a spanwise variation into the riblet geometry, so that riblets form sinusoidal waves rather than straight lines (see figure 2). Two other parameters are therefore introduced by changing the shape of the riblets, amplitude a and wavelength λ of the sinusoidal shape function. Identifying an optimum combination of those parameters is an important task for future research.

3 Large Eddy Simulations of Conventional Geometry

3.1 Numerical Method and Validation

Computational code used to perform LES of the riblet geometry is Code_Saturne [20] developed at

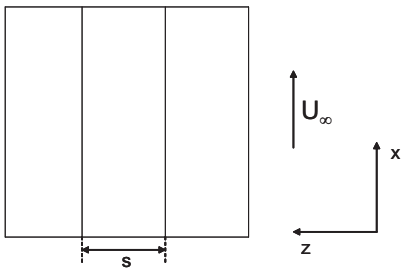

a) Conventional (straight) riblets

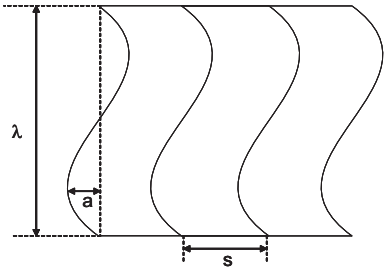

b) Proposed (sinusoidal) riblets

Figure 2: Comparison between straight and sinusoidal riblets. View from above.

Électricité de France (EDF). The code is fully conservative, second-order, unstructured finite volume solver with collocated arrangement of variables. It solves incompressible Navier-Stokes equations using fractional step method, where the pressure correction step leads to Poisson equation for pressure. The code has been used for calculation of many industrial problems in complex geometries, containing turbulence, heat transfer, combustion, two-phase flow interactions. [20].

In order to validate the code performance in application to the current problem, LES of fully-developed turbulent plane channel flow was performed by the authors of this paper using $76 \times 64 \times 64$ grid for the channel size of $2\pi\delta \times 2\delta \times \pi\delta$, where δ is the channel half-width, for Reynolds number $Re_\tau = 180$ based on friction velocity and channel half-width. Grid resolution in wall units is: $\Delta x^+ = 14$, $\Delta y^+ = 0.4 - 14$, $\Delta z^+ = 8.8$. Three eddy viscosity models are tested: Smagorinsky model with van-Driest wall functions, Smagorinsky model without wall functions and dynamic Smagorinsky model with local averaging (global averaging, i.e. averaging along the planes parallel to the wall was not implemented for purpose, since it will not be possible in the riblet case). Computational time step was kept at $\Delta t U_l/\delta = 0.05$ for all the three models. Comparison of the mean velocity and turbulent Reynolds stresses, all in wall units, with DNS of Abe et al. [21] is shown in figures 3a and 3b, respectively. It is seen right away

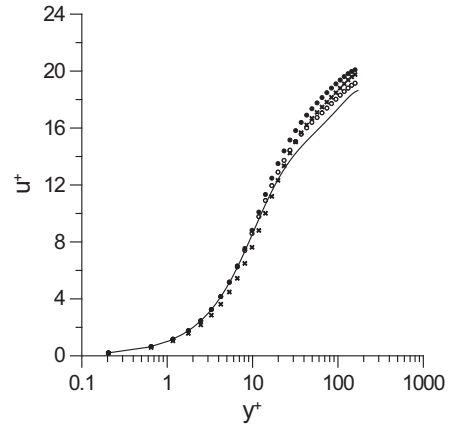

a) Mean velocity. ———, DNS [21].

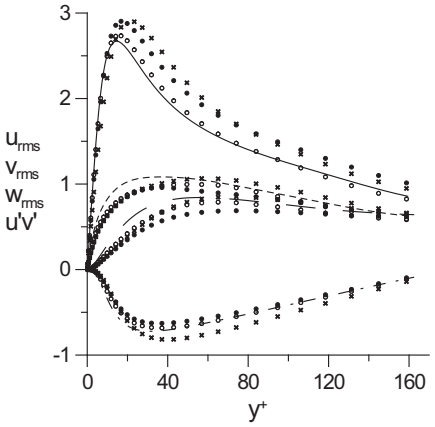

b) Reynolds stresses. Lines, DNS [21]: ———, u_{rms}; — — —, v_{rms}; − − −−, w_{rms}; — · — · —, $u'v'$.

Figure 3: Mean velocity and turbulence Reynolds stresses for the plane channel flow. ○, Smagorinsky model with wall functions; ×, Smagorinsky model without wall functions, •, dynamic model with local averaging.

that Smagorinsky model without wall functions shows the worst agreement with DNS results. Smagorinsky model with wall functions performs the best. Superiority of classical Smagorinsky model over dynamic model in this case is explained by the absence of global spanwise averaging in the dynamic model. It is known that dynamic model can produce large local negative values of Smagorinsky coefficient, which are usually smoothed by averaging. Without global averaging these negative values contaminate the results. Therefore, dynamic model might not be a good choice for three-dimensional turbulent flows.

3.2 Computational Setup

Computational domain for the riblet geometry extends $\pi\delta$ in streamwise (x) direction and $0.289\pi\delta$ in spanwise (z) direction, where δ is the half-width corresponding to the plane channel, where the riblet surface is replaced by a flat wall. The bulk Reynolds number for the calculations is $Re_b = U_b\delta/\nu = 2800$, where U_b is the bulk velocity. This Reynolds number corresponds to $Re_\tau = 180$ based on the friction velocity of the flat plate.

The bottom surface of the domain is the riblet surface, and the top surface is the flat wall. For the riblet cross-section, triangular shape is used with the riblet ridge angle $\alpha = 60\,\mathrm{deg}$ and a spanwise separation $s^+ = 20\,(s/\delta = 0.1135)$. This spanwise separation results in having eight riblets across the span of the computational domain. The computational grid has $16 \times 64 \times 128$ grid points, distributed uniformly in streamwise and spanwise directions. Grid clustering near the walls using hyperbolic tangent function is used in wall-normal direction to resolve the boundary layers. The non-dimensional grid spacing is $\Delta x^+ = 35$, $\Delta z^+ = 1.25$, minimum vertical spacing $\Delta y^+ = 0.4$ at the wall, and maximum vertical spacing $\Delta y^+ = 14$ in the middle of the channel. It is worth noting that the current numerical grid is non-orthogonal, see $y - z$ view of the grid in figure 4. Comparison of the results obtained with orthogonal and non-orthogonal grids for this configuration is planned for the near future. No-slip boundary conditions are used at the riblet surface and at the top wall, while periodic boundary conditions are employed in streamwise and spanwise directions. To account for a streamwise pressure gradient in the formulation of periodic boundary conditions, constant forcing term is introduced in a streamwise momentum equation canceling the corresponding pressure gradient term.

Computations are initialized by, first, obtaining the laminar solution, and, second, adding synthetic turbulence fluctuations to the laminar solution. Calculations are advanced with the time step $\Delta\, tU_l/\delta = 0.04$ till the computational time $tU_l/\delta = 1000$, when the statistically-steady state is achieved, after which the statistics is collected for an additional time of $tU_l/\delta = 500$. Here U_l is the centerline velocity which would occur in the laminar plane channel flow with the same bulk velocity, i.e. $U_l = 1.5\,U_b$. Reported results are obtained with Smagorinsky eddy-viscosity model with wall functions.

3.3 Results and Discussion

DNS study of the same riblet configuration [13] reported a drag reduction of 6%. To demonstrate that

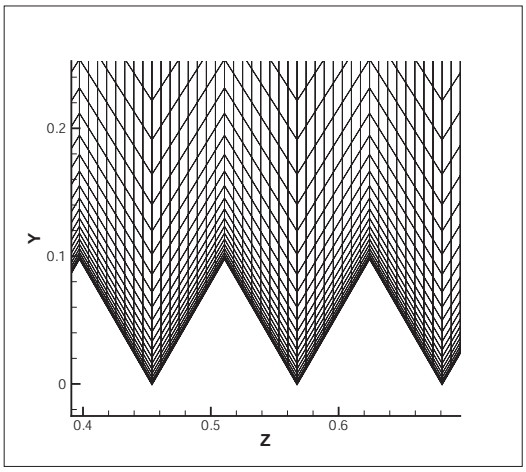

Figure 4: $y - z$ view of the numerical grid.

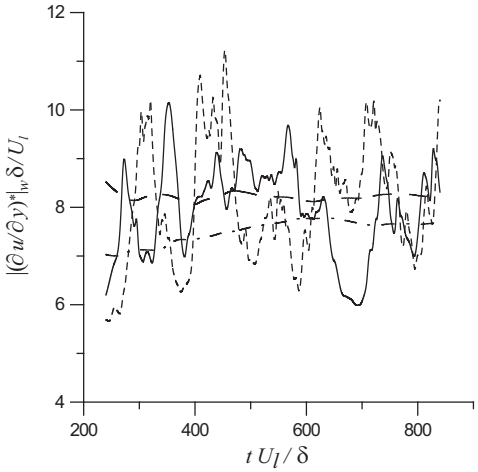

Figure 5: Time-history of effective wall-shear rates. Instantaneous: $- - - -$, at the flat surface, $(\partial\, u/\partial\, y)^*_f$; ———, at the riblet surface, $(\partial\, u/\partial\, y)^*_r$. Time-averaged: — — —, at the flat surface; — · — · —, at the riblet surface. $|\,(\partial\, u/\partial\, y)\,|_w \delta/U_l = 2$ corresponds to fully-developed laminar plane channel flow.

this configuration is indeed drag-reducing, we plot a time history of effective normalized wall-shear rates, $|\,(\partial\, u/\partial\, y)^*\,|_w\, \delta/U_l$, at the flat and riblet walls, respectively, in figure 5. Both instantaneous and time-averaged values are plotted. Time tU_l/δ in figure 5 corresponds to the normalized computational time since the beginning of accumulating statistics.

Instantaneous effective wall-shear rate $(\partial\, u/\partial\, y)^*$ is defined on the flat and riblet surfaces as

$$D_f = \mu \int_{A_f} \frac{\partial u}{\partial n}\, d\, A_f = \mu \left(\frac{\partial u}{\partial y}\right)^*_f A_f$$
$$D_r = \mu \int_{A_r} \frac{\partial u}{\partial n}\, d\, A_r = \mu \left(\frac{\partial u}{\partial y}\right)^*_r A_f, \qquad (1)$$

where A_f is the surface of the flat wall, and A_r is the surface of the riblet wall, respectively. D_f and D_r correspond to instantaneous plan-averaged drag at the flat and riblet surfaces, respectively. Figure 5 shows that instantaneous drag at the riblet surface is for the most of the time smaller than the drag at the flat surface, bringing time-averaged values to 7.69 and 8.23, respectively. This corresponds to 6.5% drag reduction, which is very close to 6% reported by Choi et al. [13] for the same configuration. Predicted time-averaged values of the normalized friction velocity u_τ/U_l at the riblet and flat surfaces are, 0.0428 and 0.0443, respectively. These values are within 3% of the values 0.0414 and 0.0430, reported by Choi et al. [13].

Lower drag observed at the riblet surface as compared to the flat surface results from the favorable interaction of riblets with the near-wall turbulence. Indeed, study of the effect of riblets on a laminar channel flow [22] showed that drag reduction was not obtained in a laminar flow. The change in a global structure of a turbulent boundary layer incurred by this favorable interaction can be demonstrated by studying the variation of the mean velocity and turbulence statistics with the spanwise location along the riblet surface. Mean velocity profiles normalized by the laminar centerline velocity, $\overline{u}/U_l$, are shown in figure 6a in comparison to DNS results of Choi et al. [13]. Results obtained with dynamic Smagorinsky model with local averaging are also plotted. Agreement with DNS results for the classical Smagorinsky model is fairly good. It can be seen that the mean velocity above the riblet valley is larger than that above the riblet tip at a given y/δ. It is consistent with the observations reported also in experimental [23] and analytical [24] studies.

Root-mean square velocity fluctuations normalized by the turbulent mean centerline velocity, U_c, compared to DNS results [13] are shown in figure 6b–d for different spanwise locations along the riblet surface. As with the mean velocity, the values of the turbulent fluctuations are higher above the riblet valley than the riblet tip for the given y/δ. Also, turbulent intensities for all three velocity components are reduced above the riblet surface compared to the same nondimensional distance from the wall in a flat plat case. Reduction is greater for the normal and spanwise velocity fluctuations than for the streamwise component, indicating that cross-flow is more sensitive to the presence of riblets than flow in the streamwise direction. Again, agreement with DNS is very favorable for the classical Smagorinsky model with wall functions. It is

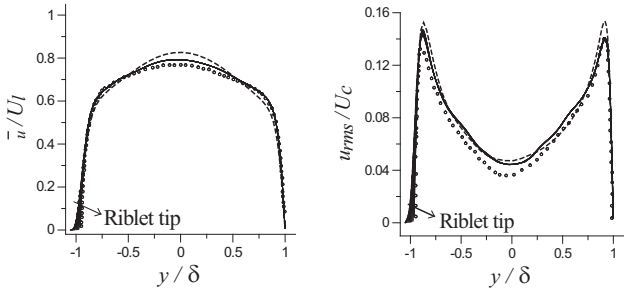

(a) Mean streamwise velocity

(b) Streamwise velocity fluctuations

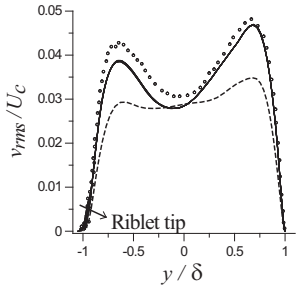

(c) Normal velocity fluctuations

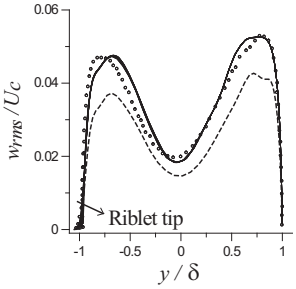

(d) Spanwise velocity fluctuations

Figure 6: Turbulence statistics for different spanwise locations along the riblet surface. ———, LES, Smagorinsky model with wall functions; – – ––, LES, dynamic model with local averaging; ∘, DNS of Choi et al. [13].

interesting to note that the dynamic model with local averaging significantly underpredicts wall-normal and spanwise velocity fluctuations. It once again shows an inferiority of the local averaging procedure with dynamic models.

It can be seen that the agreement between the two solutions is rather good.

3.4 Drag Reduction Mechanism

Reduction of turbulent fluctuations by riblets demonstrated above signifies a decrease in a turbulent momentum transfer above the riblet surface and, as a consequence, decrease in turbulent shear stresses and, finally, skin-friction drag. However, exact mechanisms explaining why the turbulence is suppressed by the presence of riblets proposed in the open literature can be divided into two groups. One group postulates that riblets impede the cross-flow motion by hampering the fluctuating cross-flow component w'. This leads to the reduction in a turbulent momentum transfer close to the wall, and, finally, decrease in the turbulent shear stress. Robinson [25] hypothesized that riblets impede the cross-stream flow necessary to replace the near wall fluid that is ejected during turbulence production events. Bechert [19] introduced a so-called "protrusion height" which is basically a geometrical property of any specific riblet configuration, and related the protrusion height to the ability of riblets to impede cross-flow. Another group states that interaction of riblets with quasistreamwise vortices is responsible for drag reduction. Quasistreamwise vortices are associated with creation of high skin friction zones in a turbulent boundary layer by bringing high-speed fluid towards the wall during the turbulent sweep events [26, 27]. Hypothesis of Choi [27] is a compromise between the two groups: he thinks that riblets restrain the cross-flow motion of the streamwise vortices, thus reducing the skin-friction. Choi et. al. [13] propose a mechanism, by which streamwise vortices are displaced by riblets further from the wall. They explain the decrease of performance for the riblets with $s^+ > 25$ by the ability of streamwise vortices to fit between the larger spaced riblet tips. Their theory is based on assumption that the typical diameter of the streamwise vortices is $d^+ \sim 30$. Pollard [28] agrees that riblets effectively displace the turbulence production events (sweeps and ejections) away from the wall, resulting in the reduced wall shear stress.

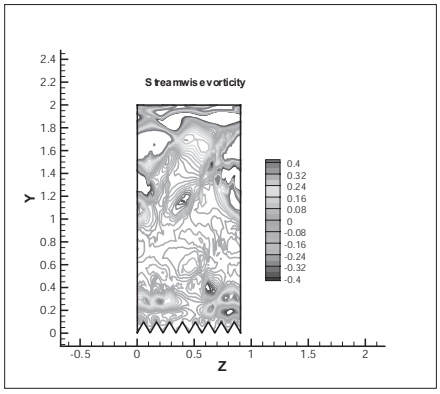

Figure 7: Spanwise view of instantaneous streamwise vorticity.

Current results support the second mechanism by showing that quasistreamwise vortices are indeed displaced away from the riblet surface compared to the flat wall (see figure 7 showing the spanwise view of instantaneous streamwise vorticity). Three-dimensional view of coherent vortical structures identified by Q-criterion and displayed in figure 8 once again confirms the reduction of turbulent activity next to the riblet surface. Displacement of streamwise vortices further from the riblet surface, suppression of their spanwise meandering and overall reduction in the amount of vortices are evident.

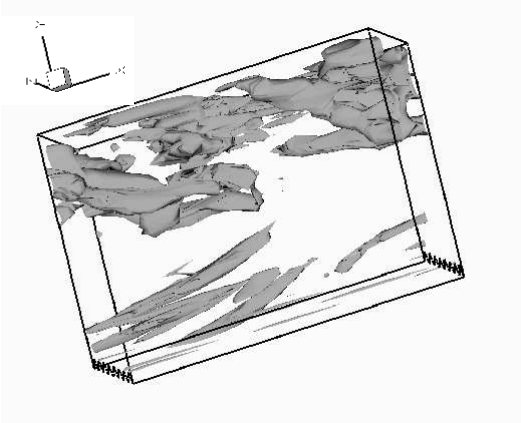

Figure 8: Coherent vortical structures identified by Q-criterion.

4 Simulations of Modified Geometry

The modified geometry is obtained from a conventional geometry described in the previous section by changing the shape of the riblets in spanwise direction from straight lines to sinusoidal waves as demonstrated in figure 2. The new shape can be described by the following equation

$$z'(x) = a\,\sin(\frac{2\,\pi}{\lambda}\,x), \tag{2}$$

where $z'(x)$ is the deviation of the spanwise coordinate of the riblet surface from the corresponding coordinate of the straight riblet. In the current simulations, we use the amplitude $a/\delta = 0.1$ and the wavelength $\lambda/\delta = \pi$ in equation (2), which gives the ratio $a/\lambda = 0.03$ and the maximum sinusoidal slope of $(dz'/dx)_{max} = 2\,\pi\,a/\lambda = 0.2$ corresponding to an angle of $11.3°$. All other parameters of the problem are left unchanged. Three-dimensional view of the computational domain is shown in figure 9. Laminar flow calculations are carried out for the same Reynolds number $Re = 2800$ based on the bulk velocity, or $Re = 4200$ based on the centerline velocity, as the straight riblet simulations. Longitudinal view of spanwise velocity developed over the sinusoidal riblet surface and normalized with the streamwise centerline velocity, w/U_l, is shown in figure 10 ($x - y$ cross-section taken through the riblet valley is plotted). An oscillatory motion of the mean flow is evident, signified by the change of the sign of spanwise velocity w in the riblet surface boundary layer from negative to positive and back to negative with the streamwise distance. If we plot spanwise velocity profiles $w(x)$ for several distances from the wall y/δ (figure 11a), we can notice that spanwise velocity distributions in the riblet surface boundary layer follow the shape of the sinusoidal slope dz'/dx. This is natural, since spanwise velocity induced by the rotation of the mean velocity vector due to the wavy motion is proportional to the slope.

By analogy with the flow near an oscillating wall, a crossflow boundary layer is developed, which confines three-dimensional effects to the layer of some finite thickness. In order to predict crossflow layer thickness and maximum spanwise velocity for any given riblet configuration, a theoretical approach based on an analogy with the Stokes layer is proposed. Stokes layer is an analytical solution of the Navier-Stokes equations for the case when a flat plate oscillates tangentially in a still fluid described by Schlichting [29]. Although it is a different phenomenon, an analogy can be followed if one takes a lagrangian approach and moves with the fluid particle in a crossflow boundary layer, which indeed follow and oscillatory trajectory. To make a comparison with the Schlichting solution, one can write an oscillation period as $T = \lambda/u^\star$, where $u^\star$ is some characteristic velocity of streamwise motion in a crossflow boundary layer. We approximate $u^\star$ as the streamwise velocity of the plane laminar channel flow at y location where the Stokes layer vorticity is maximum, i.e. at the distance of $y^\star \sim \delta_s/4$ (see [29, 30]), where

$$\delta_s = \pi\sqrt{2\,\nu/\omega} \tag{3}$$

is the Stokes layer thickness (defined here as one half of the "penetration depth" in [29]), $\omega = 2\,\pi/T$.

Taking into account that the Stokes layer thickness is small compared to the channel half-width for the considered Reynolds number, one can approximate $u^\star$ using a linear relationship derived from the analytical solution for the plane Poiseuille flow valid for small distances from the wall: $u^\star/U_l \sim 2\,y^\star/\delta = \delta_s/2\,\delta$, where U_l is the laminar centerline velocity and δ is the channel half-width. Therefore, expanding definition of $\omega = 2\,\pi/T = 2\,\pi\,u^\star/\lambda$ as

$$\omega = \frac{\pi\,U_l\,\delta_s}{\lambda\,\delta} \tag{4}$$

and substituting equation (3) for the Stokes layer thickness δ_s, one can solve for ω:

$$\omega = \sqrt[3]{\pi^4\,2\,\nu\left(\frac{U_l}{\lambda\,\delta}\right)^2} \tag{5}$$

This formula can be expected to hold only for small amplitudes a/λ of the sinusoidal riblet shape, since $u^\star$ is estimated assuming that the spanwise crossflow motion does not influence the mean streamwise velocity. For large amplitudes, spanwise oscillatory motion will most likely affect the streamwise velocity in

the crossflow boundary layer, resulting in smaller effective velocity $u^\star$ and smaller oscillation frequency than the one predicted by equation (5). For the current simulation parameters, the value of non-dimensional frequency $\omega\,\delta/U_l = 0.17$ is obtained, which allows to estimate the crossflow boundary layer thickness $\delta_s/\delta = 0.16$ from equation (3), which is the correct estimate according to the figure 10. According to Shclichting [29], spanwise velocity in a Stokes layer scales with the "wall speed" w_0, or maximum amplitude of the wall velocity. In a riblet crossflow boundary layer, similar parameter would be the spanwise velocity induced by the rotation of a characteristic velocity $u^\star$ to an angle corresponding to the local slope (dz'/dx). For small amplitudes a/λ, this can be approximated as

$$w_0\,(x) = u^\star(dz'/dx) = a\,\omega\,cos(\frac{2\,\pi\,x}{\lambda}) \qquad (6)$$

(see also equation (2)).

Note that the Stokes layer in a wall-oscillating case and a riblet crossflow boundary layer developed in the current case, in spite of their analogy, are different in nature. Stokes layer is time-dependent, whereas current crossflow layer is stationary. Also, spanwise wall velocity is oscillating in the Stokes layer, whereas it is always zero in the current case due to the no-slip conditions. Therefore, if we want to compare spanwise velocity distribution with that of a Stokes layer, we should only consider the Stokes layer profiles corresponding to the zero wall velocity, i.e. oscillation phases $\omega\,t = \pi/2$ or $\omega\,t = 3\,\pi/2$. Comparison of the spanwise velocity profiles $w/w_0(\eta)$, where $\eta = y\,\sqrt{\omega/(2\,\nu)}$ is the similarity variable, with the Stokes layer solution taken at $\omega\,t = \pi/2$, when the wall velocity is zero, is plotted in figure 11b. For comparison, we chose four different streamwise locations along the computational domain corresponding to x/λ =0, 0.13, 0.5 and 0.64. Note that w_0 calculated with equation (6) can achieve both positive and negative values, which explains why all the scaled profiles fall on a single curve for both positive and negative spanwise velocities in a crossflow layer (cf. figure 10). Although these are not the same phenomena, the similarity of the corresponding spanwise velocity profiles is striking, signifying that the viscous mechanisms responsible for the creation of boundary layers in these two cases are the same. It also shows that the crossflow boundary layer thickness δ_s and the amplitude of spanwise velocity oscillations $w_0(x)$ are estimated correctly by the current theoretical approach. It is worth noting that the maximum spanwise velocity w_{max} achieved in the current simulations can be predicted as $w_{max} = 0.3\,w_{0\,max} = 0.3\,a\omega$ (see also equation (6)). This leads to $w_{max} = 0.0051\,U_l$, which

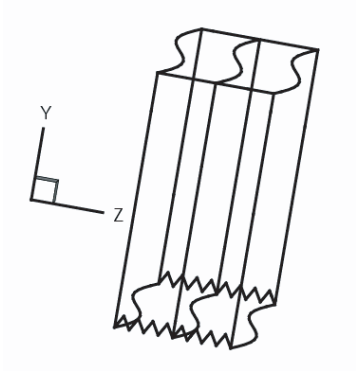

Figure 9: Three-dimensional view of the computational domain for the modified riblet geometry.

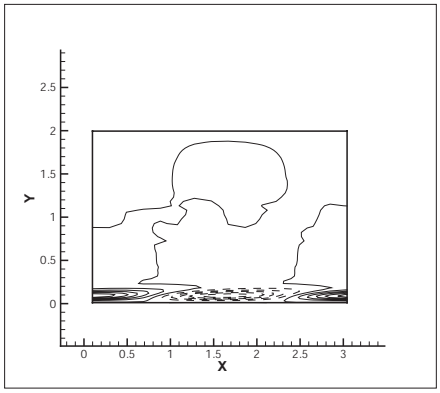

Figure 10: Longitudinal view of spanwise laminar velocity, w/U_l. Solid lines – positive values, dashed lines - negative. Velocity range: -0.005 to 0.005, contour increment: 0.001.

corresponds exactly to the maximum values observed in the simulations, see figure 10. This analysis shows that, first, a similarity between the riblet crossflow layer and a Stokes layer is established, and, second, that the current theory allows to construct correct relationship between the wavelength of the riblet shape λ and the period of the wall oscillation T in a laminar case.

Comparison of the geometrical parameters of the current simulations with the optimum parameters found in experiments of Choi et al. [30, 31] on turbulent drag reduction with spanwise oscillating wall, where maximum drag reduction of about 40% was obtained, is summarized in Table 1, all in wall units. Although the Stokes layer thickness and the period of oscillations are of the same order, the spanwise velocity amplitude $w^+_{0\,max}$ determining the maximum spanwise velocity and, therefore, an amount of vorticity introduced by the Stokes layer, is much smaller in the current simulations. The influence of this disparity on the drag reduction properties shall be investigated.

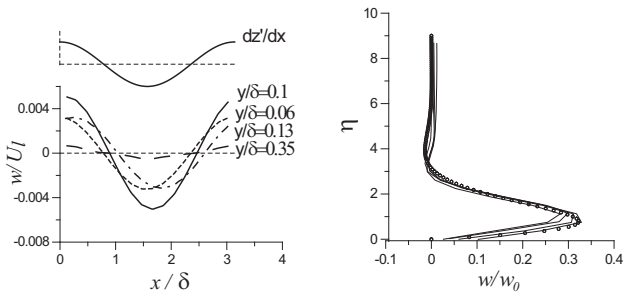

(a) Streamwise profile, $w(x)$, for several distances from the wall, y/δ. Slope of the riblet surface, dz'/dx, is also shown.

(b) Vertical profile, $w(\eta)$. Lines, computations; symbols, analytical solution [29]

Figure 11: Laminar spanwise velocity profiles over the sinusoidal riblet surface.

Table 1: Comparison of geometrical parameters of the current simulations with the optimum parameters in experiments of Choi et al. [30, 31]

	Simulations	Experiments
δ_s^+	28.8	30
$w_{0\,max}^+$	0.4	15
T^+	285	100

5 Conclusion

A new modification to the conventional drag reduction method using riblets is proposed. The modified riblet configuration is obtained from the conventional one by adding a sinusoidal variation to the riblet shape in spanwise direction. We hope that this modification will increase an amount of drag reduction, since the mean flow will resemble the flow occurring during the spanwise-wall oscillation, which was recently discovered to offer significant drag reduction. Large Eddy Simulations of the conventional riblet geometry is performed with the purpose of validating the numerical method to be used for sinusoidal riblet computations. It is also important to understand the mechanism of drag reduction in a simpler case of straight riblets before studying sinusoidal riblets. LES results are compared with DNS of Choi et al. [13] and good quantitative agreement is obtained for Smagorinsky model with wall functions. Computations of the sinusoidal riblets are performed in the laminar regime, and resulting mean flow is documented and analyzed. An analytical approach is proposed to relate the wavelength of the riblet shape λ with the period of oscillations T in a laminar regime. Analogy of the mean flow over the sinusoidal riblet surface with the flow which occurs during the spanwise wall oscillation is confirmed. Non-dimensional parameters leading to an optimized drag-reducing configuration with wall oscillations are compared with the parameters of the current simulations. Although the period of oscillations and the thickness of the Stokes layer are of the same order of magnitude, smaller amplitude of spanwise velocity is observed.

Acknowledgements: This work is supported by Agence Nationale pour la Recherche (project PAN-H/READY).

References:

[1] C. E. Wooldridge and R. I Muzzy. Boundary layer turbulence measurements with mass addition and combustion. *AIAA J.*, 4:2009–2016, 1966.

[2] M. R. Malik, L. M. Weinstein, and M. Y. Hussaini. Ion wind drag reduction. AIAA Paper 83–0231, 1983. New York.

[3] J. L. Lumley. Drag reduction in turbulent flow by polymer additives. *J. Polymer Sci. Macromol. Rev.*, 7:263, 1973.

[4] P. S. Virk. Drag reduction fundamentals. *AIChE J.*, 21:625, 1975.

[5] P. V. Aslanov, S. N. Maksyutenko, I. L. Povkh, A. P. Simonenko, and A. B. Stupin. Turbulent flows of solutions of surface-active substances. *Izvestiya Akademii Nauk SSSR, Mekhanika Ghidkosti i Gaza*, 1:36–43, 1980.

[6] M. Gad el Hak. Compliant coatings for drag reduction. *Prog. Aerospace Sci.*, 38:77–99, 2002.

[7] C. L. Merkle and S. Deutsch. Microbubble drag reduction. In *Frontiers in Experimental Fluid Mechanics*, ed. M. Gad-el-Hak, pages 291–336. Springer-Verlag, New York, 1989.

[8] J. W. Hoyt. Turbulent flow of drag-reducing suspensions. Technical Report No. TP 299, 1972. Naval Undersea Center, San Diego, California.

[9] I. Radin. *Solid-Fluid Drag Reduction*. PhD thesis, University of Missouri, Rolla, Missouri, 1974.

[10] T. C. Corke, Y. Guezennec, and H. M. Nagib. Modification in drag of turbulent boundary layers resulting from manipulation of large-scale structures. In *Viscous Flow Drag Reduction*, ed.

G. R. Hough, pages 128–143. AIAA, New York, 1980.

[11] J. B. Anders. Outer-layer manipulations for turbulent drag reducion. In *Viscous Drag Reduction in Boundary Layers*, eds. D. M. Bushnell and J. N. Heffner, pages 263–284. AIAA, Washington, D.C., 1990.

[12] M. J. Walsh. Riblets. In *Viscous Drag Reduction in Boundary Layers*, eds. D. M. Bushnell and J. N. Heffner, pages 203–261. AIAA, Washington, D.C., 1990.

[13] H. Choi, P. Moin, and J. Kim. Direct numerical simulation of turbulent flow over riblets. *J. Fluid Mech.*, 255:503–539, 1993.

[14] L. Sirovich and S. Karlsson. Turbulent drag reduction by passive mechanisms. *Nature*, 388(21):753–755, 1997.

[15] W. J. Jung, N. Mangiavacchi, and R. Akhavan. Suppression of turbulence in wall bounded flows by high-frequency spanwise oscillations. *Phys. Fluids*, 8:1605–1607, 1992.

[16] K.-S. Choi, J. R. DeBisschop, and B. R. Clayton. Turbulent boundary-layer control by means of spanwise-wall oscillation. *AIAA J.*, 36:1157, 1998.

[17] M. Gad-El-Hak. *Flow Control*. Cambridge University Press, 2000.

[18] A. Baron and M. Quadrio. Turbulent boundary layer over riblets: Conditional analysis of ejection-like events. *Int. J. Heat and Fluid Flow*, 18:188–196, 1997.

[19] D. W. Bechert, M. Bruse, W. Hage, J. G. T. Van Der Hoeven, and G. Hoppe. Experiments on drag-reducing surfaces and their optimization with an adjustable geometry. *J. Fluid Mech.*, 338:59–87, 1997.

[20] F. Archambeau, N. Méchitoua, and M. Sakiz. Code_saturne: a finite volume code for the computation of turbulent incomressible flows - industrial applications. *Int. J. Fin. Vol.*, 1, 2004.

[21] H. Abe, H. Kawamura, and Y. Matsu. Direct numerical simulation of a fully developed turbulent channel flow with respect to reynolds number dependence. *ASME Journal of Fluids Engineering*, 123:382, 2001.

[22] H. Choi, P. Moin, and J. Kim. On the effect of riblets in fully developed laminar channel flow. *Phys. Fluids*, page 1892, 1991.

[23] A. Hooshmand, R. A. Youngs, J. M. Wallace, and J.-L. Balint. An experimental study of changes in the structure of a turbulent boundary layer due to surface geometry changes. AIAA Paper 83-0230, 1983. New York.

[24] D. W. Bechert and M. Bartenwerfer. The viscous flow on surfaces with longitudinal ribs. *J. Fluid Mech.*, 206:105–129, 1989.

[25] S. K. Robinson. Coherent motions in the turbulent boundary layer. *Ann. Rev. Fluid Mech.*, 23:601, 1991.

[26] H. Choi, P. Moin, and J. Kim. Turbulent drag recution: Studies of feedback control and flow over riblets. TF-55 83-0230, 1992. Department of Mechanical Engineering. Stanford University, Stanford, California.

[27] K.-S. Choi. Near-wall structure of a turbulent boundary layer with riblets. *J. Fluid Mech.*, 208:417–458, 1989.

[28] A. Pollard. Passive and active control of near-wall turbulence. *Prog. Aerospace Sci.*, 33:689–708, 1997.

[29] H. Schlichting. *Boundary-layer theory*. Berlin; New York: Springer, 8 rev. and enl. edition, 2000.

[30] K.-S. Choi and B. R. Clayton. The mechanism of turbulent drag reduction with wall oscillation. *Int. J. Heat and Fluid Flow*, 22:1–9, 2001.

[31] K.-S. Choi. Near-wall structure of turbulent boundary layer with spanwise-wall oscillation. *Phys. Fluids*, 14(7):2530–2542, 2002.